Journal of Nuclear Materials 379 (2008) 162–168

Contents lists available at ScienceDirect

Journal of Nuclear Materials

journal homepage: www.elsevier.com/locate/jnucmat

Electrochemical impedance spectroscopic study of passive zirconium

Jiahe Ai [a], Yingzi Chen [a], Mirna Urquidi-Macdonald [b], Digby D. Macdonald [a,*]

[a] Center for Electrochemical Science and Technology, Department of Materials Science and Engineering, Pennsylvania State University, University Park, PA 16802, USA
[b] Department of Engineering Science and Mechanics, Pennsylvania State University, University Park, PA 16802, USA

A B S T R A C T

Spent, unreproccessed nuclear fuel is generally contained within the operational fuel sheathing fabricated from a zirconium alloy (Zircaloy 2, Zircaloy 4, or Zirlo) and is then stored in a swimming pool and/or dry storage facilities until permanent disposal in a licensed repository. During this period, which begins with irradiation of the fuel in the reactor during operation, the fuel sheathing is exposed to various, aggressive environments. The objective of the present study was to characterize the nature of the passive film that forms on pure zirconium in contact with an aqueous phase [0.1 M $B(OH)_3$ + 0.001 M LiOH, pH 6.94] at elevated temperatures (in this case, 250 °C), prior to storage, using electrochemical impedance spectroscopy (EIS) with the data being interpreted in terms of the point defect model (PDM). The results show that the corrosion resistance of zirconium in high temperature, de-aerated aqueous solutions is dominated by the outer layer. The extracted model parameter values can be used in deterministic models for predicting the accumulation of general corrosion damage to zirconium under a wide range of conditions that might exist in some repositories.

1. Introduction

The disposal of high level nuclear waste (HLNW) represents one of the greatest scientific and technological challenges [1,2], and the corrosion resistance of fuel cladding materials (generally the zirconium alloys Zircaloy 2, Zircaloy 4, and Zirlo) plays a key role during irradiation in the reactor during operation, during storage in swimming pool spent fuel storage facilities (including dry storage) and if the containers should be breached in a disposal repository. Accordingly, a detailed knowledge of the corrosion behavior of zirconium is essential for evaluating zirconium alloy behavior and for ultimately predicting the probability that the cladding will be breached either during irradiation or during storage. However, to date, little effort has been made to develop deterministic models that are based on sound electrochemical principles for predicting the accumulation of corrosion damage and containment performance under extreme HLNW repository conditions. The objective of this work is to optimize the PDM on experimental electrochemical impedance spectroscopy (EIS) data and to extract values for various model parameters. In this system, the passive film comprises a non-porous, defective oxide barrier layer (ZrO_{2-x}) and a precipitated, porous oxide outer layer. We have employed a different method of formulating the model form that employed previously [1] and, using an unconstrained optimization procedure, we have extracted values for the individual parameters in the PDM bi-layer model that are physically eminently reasonable.

2. Experimental procedures

A controlled hydrodynamic apparatus that was previously developed [3] for performing electro-chemical and corrosion studies in high-temperature aqueous systems was used to carry out all electrochemical experiments reported in this study. The three-electrode test cell comprised a 600 mL reactor containing a magnetically activated impeller, a thermocouple, a working electrode, a counter electrode, a reference electrode, and an annular flow channel. The working electrode was fabricated from polycrystalline zirconium rod from Alfa Acer and had an exposed surface area of 5.82 cm^2. The sample was abraded with 800 and 1200 grit SiC paper, and then further polished with 3 μm and 1 μm diamond paste one day before an experiment. The zirconium rod used in this study contained 0.25 wt% Sn, 0.01 wt% Ni, 0.11 wt% Fe, and 0.01 wt% Cr, bal Zr, as determined by electron probe micro analysis (EPMA). An insulated Type 316 L SS wire was connected to the bottom of the annular flow channel and then taken out through the top of the vessel via an insulated pressure fitting, with the whole channel serving as the counter electrode. The reference electrode was a saturated silver/silver chloride (SSCE) and all potentials were converted to the standard hydrogen electrode (SHE) scale via thermodynamic calculation. The solution comprised 0.1 M $B(OH)_3$ + 0.001 M LiOH for pH control. All experiments reported

* Corresponding author. Tel.: +1 814 863 7772; fax: +1 814 863 4718.
E-mail address: ddm2@psu.edu (D.D. Macdonald).

0022-3115/$ - see front matter © 2008 Elsevier B.V. All rights reserved.
doi:10.1016/j.jnucmat.2008.06.011

here were carried out at 250 °C and at a pressure of 62 bar (900 psi), in order to maintain a single liquid phase in the system. Passive films were grown on zirconium potentiostatically. Potentiodynamic polarization curves were measured using a positive voltage scan rate of 1 mV/s from a starting point that was 0.2 V more negative than the open circuit potential. At each potential step, in the potentiostatic film growth studies, the current was monitored as a function of time until steady state was achieved (defined as the current not changing perceptibly over 24 h). Then, the electrochemical impedance was recorded with a Solartron 1255B Frequency Response Analyzer using an excitation voltage of 10 mV (peak-to-peak) and an applied frequency from 100 kHz to 0.01 Hz. All EIS data were measured in the ascending voltage direction.

3. Impedance model

As a result of careful review of the literature, the PDM has been modified by noting that the passive film that forms on zirconium under de-aerated aqueous solution conditions comprises an outer, porous oxide layer overlying a defective oxide (ZrO_{2-x}) barrier layer. Mott–Schottky analysis shows that the film displays *n*-type electronic character, indicating a preponderance of oxygen vacancies and/or zirconium interstitials in the barrier layer [4]. Fig. 1 displays the interfacial defect generation and annihilation reactions that are envisioned to occur in the system, together with barrier layer dissolution and outer layer formation and dissolution. Thus, Reaction (1) is responsible for the injection of the interstitial Zr_i^{4+} into the barrier layer at the metal/barrier layer interface (MBI). The interstitial ion is then transmitted through the barrier layer and is ejected into the outer layer as described by Reaction (3). Reaction (2) leads to the growth of the barrier layer into the metal substrate, and Reaction (5) results in the destruction of the barrier layer by dissolution. Reaction (4) describes oxygen vacancy annihilation by oxygen ion injection at the barrier layer/outer layer interface (BOI). Note that Reactions (1), (3), and (4) are lattice-conservative processes, as they do not result in the movement of the interface with respect to a laboratory frame of reference, whereas Reactions (2) and (5) are non-conservative. A steady state must involve at least two non-conservative reactions, since only one non-conservative reaction would lead to monotonic growth or thinning of the passive film. Reactions (6) and (7) correspond to the formation and dissolution of the outer layer. Note that Fig. 1 is not scaled. The thickness of the barrier layer is on the order of nanometers, whereas the outer layer may have a much greater thickness (up to a 100 μm) [5]. Note that Reaction (6), corresponding to the precipitation of ZrO_2, is envisaged to occur at the interface between the barrier and outer layers of the passive film, most likely within the pores in the outer layer. The pores do not become filled with zirconium oxide, because of the dependence of the Gibbs energy of the pore wall on curvature (Gibbs–Thompson effect). Further note that Reaction (7) is simply not the reverse of Reaction (6), because it is envisaged to occur at the outer surface of the outer layer and perhaps within the outer reaches of the pore. Accordingly, these processes are spatially separated and, hence, are properly considered to be separate processes.

The reaction rate constants, k_j, are functions of the potential drops across the two interfaces, and may be functions of the potential drops across the barrier and outer layers, and the barrier layer thickness, L_{bl}, and the pH at the BOI [1]. In any event, the potential applied at the BOI is related to the potential applied across the entire system, *V*, and the potential drop across the outer layer, $I \cdot R_{ol}$. The rate constants can then be written from activated complex theory as

$$k_i = k_i^0 \cdot e^{a_i \cdot (V - I \cdot R_{ol})} \cdot e^{b_i L_{bl}} \cdot e^{c_i \cdot pH_{BOI}} \quad (i = 1, 2, 3, 4, 5), \tag{1}$$

where $a_5 = 0$; b_3, b_4 and b_5 are all equal to zero.

The unknown rate constants for the five primary interfacial reactions are shown in Table 1. Note that only the rate constants for the reactions that occur at the MBI [Reactions (1) and (2)] are functions of the thickness of the barrier layer and that all of the rate constants, except that for the non-electrochemical Reaction (5), are functions of the applied voltage, *V*, and the voltage drop across the outer layer ($I \cdot R_{ol}$).

All interfacial reactions that produce or consume electrons contribute to the total current density under anodic polarized conditions, *I*.

$$I = 4F \cdot [k_1 + k_2], \tag{2}$$

where *F* is Faraday's constant.

In order to simplify the model further, we assume that the pH at BOI is a constant, and hereinafter we merge $e^{c_i \cdot pH}$ into k_i^0. Note that the total current density is a function of *V*, and L_{bl}. (Note also that R_{ol} is regarded as being a constant under steady-state conditions.) Accordingly, for any arbitrary changes δV, and δL_{bl}, and by assuming that the porosity of the outer layer, *P*, is also a constant, we write the total differentials of Eqs. (1) and (2) as follows:

$$\delta I = 4F \cdot [\delta k_1 + \delta k_2] \tag{3}$$

and

$$\delta k_i = a_i k_i \delta V + b_i k_i \delta L_{bl} - a_i k_i R_{ol} \delta I. \tag{4}$$

Substitution of Eq. (4) into Eq. (3) yields

$$\delta I = 4F[(a_1 k_1 + a_2 k_2)\delta V + (b_1 k_1 + b_2 k_2)\delta L_{bl} - (a_1 k_1 + a_2 k_2) R_{ol} \delta I]. \tag{5}$$

The variations in *I*, *V*, and L_{bl} are sinusoidal in an EIS measurement, so that we can write like that

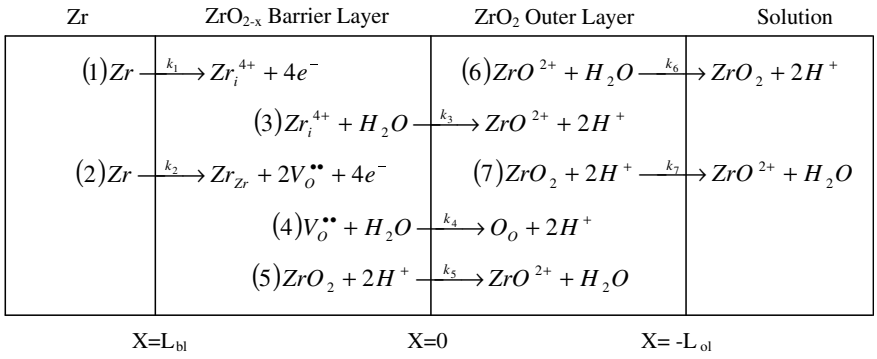

Fig. 1. Interfacial reactions leading to generation and annihilation of point defects within the passive film on a zirconium surface. Zr = zirconium atom, Zr_i^{4+} = metal interstitial in the barrier layer, Zr_{Zr} = zirconium cation in a normal cation site on the metal sub-lattice in the barrier layer, $V_{\ddot{O}}$ = oxygen anion vacancy on the anion sub-lattice of the barrier layer, O_O = oxygen ion in a normal site on the oxygen sub-lattice of the barrier layer.

Table 1
Rate constant $k_i = k_i^0 e^{a_i(V-IR_{ol})} e^{b_i L}$ for interfacial reactions based on the point defect model

Interfacial reactions	a_i (V^{-1})	b_i (cm^{-1})	k_i^0 (cm/s)
(1) $Zr \xrightarrow{k_1} Zr_i^{4+} + 4e^-$	$4\alpha_1(1-\alpha)\gamma$	$-4\alpha_1\gamma\cdot\varepsilon$	$k_1^{00} e^{-4\alpha_1\cdot\gamma\cdot(\phi^0_{BOI}+\beta\cdot pH)}$
(2) $Zr \xrightarrow{k_2} Zr_{Zr} + 2V_o^{\cdot\cdot} + 4e^-$	$4\alpha_2(1-\alpha)\gamma$	$-4\alpha_2\gamma\cdot\varepsilon$	$k_2^{00} e^{-4\alpha_2\cdot\gamma\cdot(\phi^0_{BOI}+\beta\cdot pH)}$
(3) $Zr_i^{4+} + H_2O \xrightarrow{k_3} ZrO^{2+} + 2H^+$	$4\alpha_3\alpha\gamma$	0	$k_3^{00} e^{4\alpha_3\cdot\gamma\cdot(\phi^0_{BOI}+\beta\cdot pH)}$
(4) $V_o^{\cdot\cdot} + H_2O \xrightarrow{k_4} O_o + 2H^+$	$2\alpha_4\alpha\gamma$	0	$k_4^{00} e^{2\alpha_4\cdot\gamma\cdot(\phi^0_{BOI}+\beta\cdot pH)}$
(5) $ZrO_2 + 2H^+ \xrightarrow{k_5} ZrO^{2+} + H_2O$	0	0	k_5^{00}

where $\gamma = F/RT$; $\alpha = d\Phi_{BOI}/dV$; $\beta = d\Phi_{BOI}/dpH$.

$$\delta X = \Delta X \cdot e^{j\cdot\omega\cdot t}, \tag{6}$$

where X represents I, V, or L_{bl}. Substitution of Eq. (6) into Eq. (5) divided by δV yields the Faradic admittance Y_f

$$Y_f = \frac{4F(a_1k_1 + a_2k_2)}{S_0} + \frac{4F(b_1k_1 + b_2k_2)}{S_0}\frac{\Delta L_{bl}}{\Delta V}, \tag{7}$$

where $S_0 = 1 + 4F(a_1k_1 + a_2k_2)R_{ol}$.

The derivation of $\Delta L_{bl}/\Delta V$ is as follows. Firstly, we write the mass balance condition for the barrier layer as

$$\frac{dL_{bl}}{dt} = \Omega\cdot k_2 - \Omega\cdot k_5(C_{H^+}^{BOI})^n, \tag{8}$$

where Ω =21.06 cc/mol is the volume per mole of cations in the barrier layer, $C_{H^+}^{BOI}$ is the concentration of hydrogen ion at the barrier layer/outer layer interface (assumed to be a constant), and n is the kinetic order of the film dissolution reaction with respect to the concentration of hydrogen ion. Taking the total differential as

$$\frac{d\delta L_{bl}}{dt} = j\omega\cdot\Delta L_{bl}\cdot e^{j\cdot\omega\cdot t} = \Omega\cdot(a_2k_2\cdot\delta V + b_2k_2\cdot\delta L_{bl} - a_2k_2R_{ol}\delta I) \tag{9}$$

we find that

$$\frac{\Delta L_{bl}}{\Delta V} = \frac{\Omega\cdot a_2k_2}{j\omega - \Omega\cdot b_2k_2} - \frac{\Omega\cdot a_2k_2R_{ol}}{j\omega - \Omega\cdot b_2k_2}\cdot Y_f. \tag{10}$$

Substitution of Eq. (10) into Eq. (7) yields the Faradic admittance Y_f

$$Y_f = \frac{4F\Omega\cdot a_2k_2(b_1k_1 + b_2k_2) + 4F(a_1k_1 + a_2k_2)(j\omega - \Omega b_2k_2)}{4F\Omega\cdot a_2k_2R_{ol}(b_1k_1 + b_2k_2) + S_0(j\omega - \Omega b_2k_2)}. \tag{11}$$

The total impedance comprises the impedance of the barrier layer, including those of the two interfaces, Z_{bl}, and that of the barrier layer itself, in series with that of the outer layer and the resistance of the experimental system except for the passive film Z_{ol} and R_{bs}, respectively. As for the barrier layer, its impedance is the sum of four components: (a) impedance due to the Faradic process, Z_f (i.e. $1/Y_f$), (b) impedance due to geometric capacitance, $Z_{C_{bl}}$, (c) resistance due to the transport of electrons and electron holes, $Z_{e,h}$, and (d) the Warburg impedance, Z_w, due to the transport of defects within the layer. As for the outer layer, its impedance comprises the resistance, R_{ol}, due to electrolyte in the pores in parallel with an impedance due to the geometric capacitance, $Z_{C_{ol}}$. Therefore, the total impedance of the bi-layer passive film becomes

$$\begin{aligned} Z_{total} &= Z_{bl} + Z_{ol} + R_{bs} \\ &= 1/[Z_{C_{bl}}^{-1} + (Z_f + Z_w)^{-1} + Z_{e,h}^{-1}] + 1/(R_{ol}^{-1} + Z_{C_{ol}}^{-1}) + R_{bs}, \end{aligned} \tag{12}$$

where $R_{ol} = \rho\cdot L_{ol}/P$, and ρ is the resistivity of the solution in the outer layer pores. For sufficiently high frequencies ($f > 10^{-5}$ Hz), the Warburg impedance can be written as $Z_w = \sigma/\sqrt{\omega} - j\sigma/\sqrt{\omega}$ [6], where σ and ω are Warburg coefficient and angular frequency, respectively.

4. Results and discussion

4.1. Validity of the measured impedance data

Electrochemical impedance spectra (EIS) for the passive films on zirconium were measured over a wide range of frequencies (typically 100 kHz to 0.01 Hz) as a function of the formation potential across the passive range in 0.1 M $B(OH)_3$ + 0.001 M LiOH solutions (pH 6.94 at 250 °C). The impedance was measured after holding the potential constant at each point for 24 h, in order to ensure that the passive film exists in the steady state, as determined by the constancy of the current. The measurements were carried out in the ascending potential direction. Since the stability of the electrochemical system during the EIS measurements is critical to obtaining viable data, the quality of the EIS data was checked both experimentally and theoretically. The data were checked experimentally by stepping the frequencies from high-to-low and then immediately back from low-to-high, with the impedance being measured at each step, to ascertain that the same values were obtained at equivalent frequencies in the two directions. If the system is in the steady state, which means that the thickness and current are independent of time, the impedance data should match in the two frequency step directions. The Nyquist and Bode plots show that the impedance data measured in the two step directions after holding the potential at each applied potential for 24 h for the film to attain a steady state are coincident. This is a particularly good test for system stability. The quality of the impedance data was also checked using the Kramers–Kronig transforms, which indicates excellent agreement is obtained, except for the small discrepancies at low frequencies. The discrepancies are due to the 'tails' problem that arises from the fact that the impedance data are measured over a finite bandwidth whereas the transforms are defined over an infinite bandwidth in frequency.

4.2. Extraction of model parameter values from EIS data

The DataFit (Version 8.0) commercial software was used in this work for optimization, so as to obtain values for the standard rate constants, k_i^{00}, and transfer coefficients, α_i, for the i elementary interfacial reactions, the polarizability of the barrier layer/outer layer interface (BOI), α, the electric field strength across barrier layer, ε, and other parameters, as described below. Optimization was carried out in five stages. First of all, the total impedance model was decomposed into two parts for the real and imaginary components; secondly, the optimization model, together with the experimental impedance data upon which it will be optimized, needs to be carefully defined; thirdly, approximate parameter values were obtained by 'manually optimizing' the model for $Z(\omega)$ on the experimental data; fourthly, optimize the parameter values using the DataFit code; and finally, test the optimization results. The optimization procedure ends if the result satisfies the following requirements simultaneously; if not, the procedure returns to the third stage and the model is optimized once again. These requirements include: (1) all the parameter values are physically reasonable and should exist within known bounds; (2) the calculated $Z'(\omega)$ and $Z''(\omega)$ should agree with their respective experimental results in both the Nyquist and Bode planes; (3) the parameters, such as the polarizability, α, the electric field strength across barrier layer [7], ε, the standard rate constants, k_i^{00}, the transfer coefficients, α_i, and the constant, ϕ^0_{BOI}, should be approximately potential-independent; and (4) the calculated current density and passive film thickness, as estimated from the parameter

values obtained from the optimization, should be in reasonable agreement with the steady-state experimental values. Given that bulk ZrO_2 is oxygen vacant, with the oxygen vacancy being the principal point defect, and that no evidence could be found for the existence of metal interstitial, the rate constants for the interstitial generation and annihilation were set to be negligible values. Thus, the final model used in the optimization comprised Reactions (2), (4), and (5), Fig. 1.

Typical experimental impedance spectra for the passive state on zirconium in high temperature, deaerated borate buffer solution (0.1 M $B(OH)_3$ + 0.001 M LiOH aqueous solution, pH 6.94 at 250 °C) are shown in Fig. 2, in the form of Nyquist plots and Bode plots, respectively. It is important to note that the data satisfy the Kramers–Kronig transforms [8,9], demonstrating that the system complies with the constraints of linear systems theory. In this figure, the imaginary component of the impedance is plotted versus the real component in the Nyquist plane as a function of decreasing frequencies for three potentials. The data are also plotted in the form of the modulus, $|Z|$, and the phase angle, θ, (i.e. $\arctan(-Z_{imag}/Z_{real})$ versus the logarithm of the frequency. Also plotted in this figure are impedance data calculated from the model described above using the optimized model parameters. From this figure, it can be seen that the simulated data agree well with the experimental data, with the level of agreement being similar to that reported in other studies [1,10,11]. Thus, the impedance model based on the PDM provides a reasonable account of the experimental data.

The calculated thickness of the passive film (barrier + outer layers) is very close to the experimental value when the dielectric constant is taken to be the reasonable value of $\varepsilon = 31$ [12]. Likewise, the calculated current density, based on the fitting parameter values, also approaches its steady-state experimental value, I_{ss}. Furthermore, the porosity of outer layer, the resistance of solution of the experimental system, the polarizability of the BOI, electric

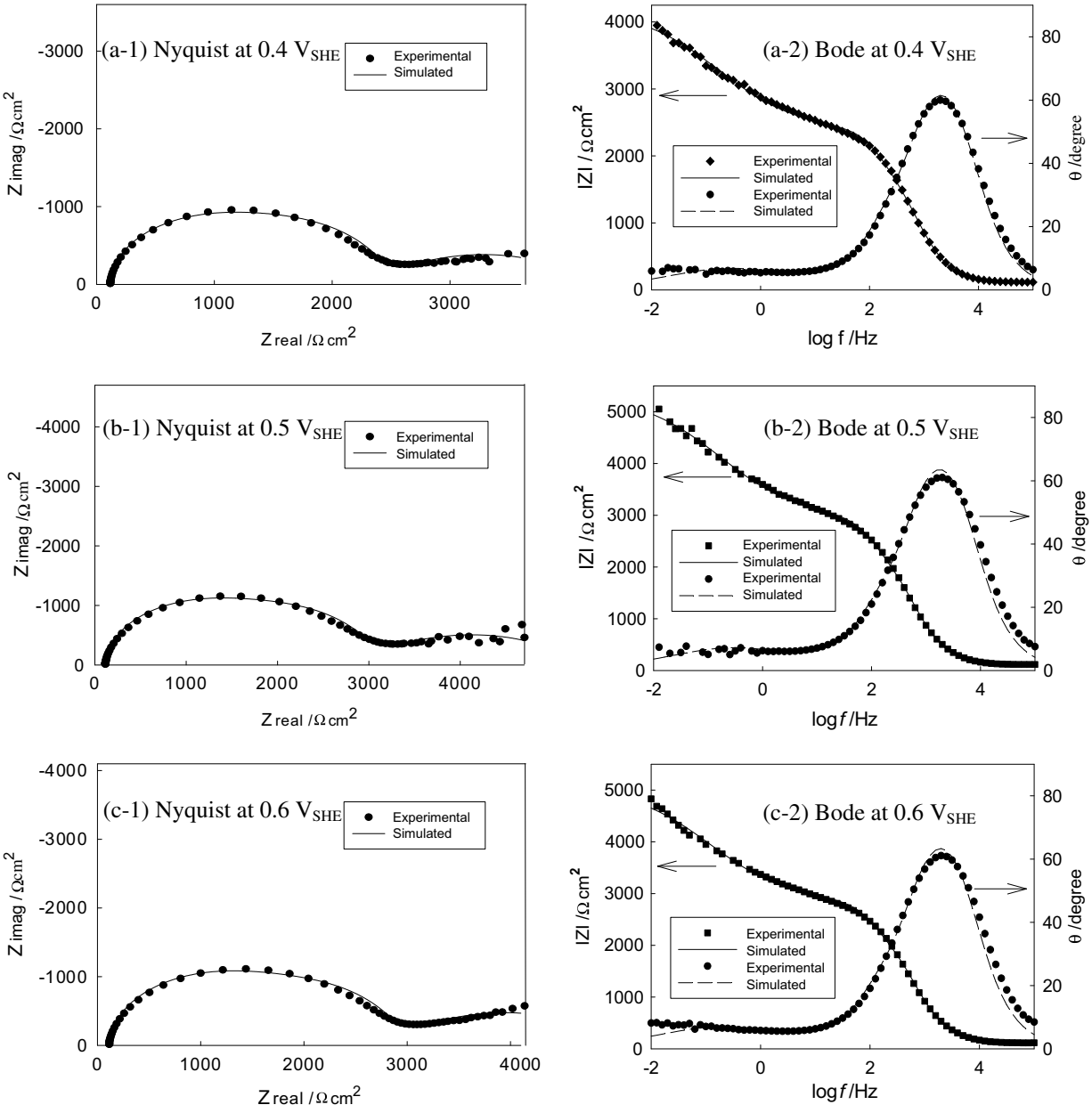

Fig. 2. Nyquist and Bode impedance plots for passive zirconium polarized for 24 h in 0.1 M $B(OH)_3$ + 0.001 M LiOH solutions at 250 °C and 62 bar and as a function of potential, showing a comparison between the experimental and simulated data.

Table 2
Parameter values after optimization of the point defect model on the experimental impedance data for zirconium in aqueous solution (pH 6.94) at 250 °C

E_{app} (V) vs. SHE	0.4	0.5	0.6	Mean (±SD)
Capacitance of barrier layer (F/cm^2)	1.01×10^{-6}	1.00×10^{-6}	1.08×10^{-6}	
Capacitance of outer layer (F/cm^2)	2.08×10^{-7}	2.09×10^{-7}	1.90×10^{-7}	
Thickness of barrier layer (cm)	1.11×10^{-7}	1.52×10^{-7}	1.61×10^{-7}	
Thickness of outer layer (cm)	1.63×10^{-5}	1.79×10^{-5}	1.82×10^{-5}	
Porosity of outer layer, P	0.396	0.373	0.387	
Resistance of solution, R_{bs} (Ω)	121.4	125.2	124.5	123.7 ± 2.3
Resistance of outer layer (Ω)	1290	1510	1550	
Warburg coefficient, σ	2990	3927	3040	$(3.32 \pm 0.60) \times 10^3$
Impedance due to electrons and holes (Ω)	2784	3697	3384	
Polarizability, α	0.188	0.195	0.194	0.192 ± 0.004
β (V)	−0.005	−0.005	−0.005	−0.005, assumed
Electric field across barrier layer, ε, (V/cm)	492 871	564 288	519 162	$(5.25 \pm 0.39) \times 10^5$
ϕ^0_{BOI} (V)	−0.243	−0.181	−0.175	−0.200 ± 0.043
Standard rate constant, k_2^{00} (mol s^{-1} cm^{-2})	2.50×10^{-15}	2.25×10^{-15}	2.52×10^{-15}	$(2.42 \pm 0.17) \times 10^{-15}$
Transfer coefficient of Reaction (2), α_2	0.277	0.271	0.262	0.270 ± 0.008

field strength across barrier layer, standard rate constants, transfer coefficients and ϕ^0_{BOI} obtained by optimization of the model on the experimental impedance data are all found to be essentially potential-independent within the applied potential range, which, in itself, is a test of the viability of the model described above. Moreover, the thickness of the barrier layer is found to increase with increasing applied potential, which is consistent with the predictions of the PDM for passive films on metals and alloys [13].

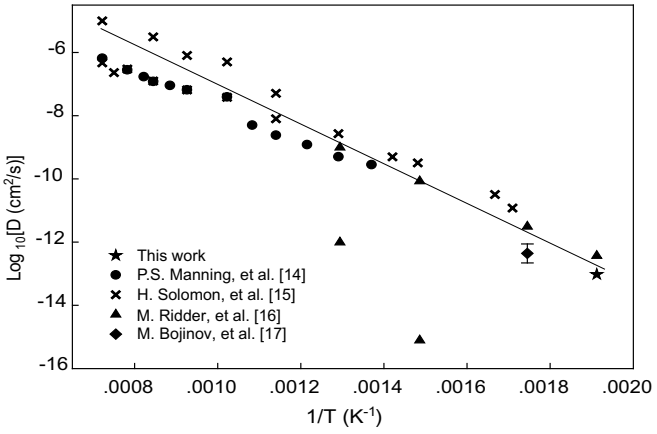

Fig. 3. Comparison of oxygen vacancy diffusivity obtained in this work and those from the literature.

The parameter values have been averaged to yield a single set for passive zirconium, which is shown in Table 2. It should be noted that the value for β was assumed to be −0.005 [1] and the assumption is due to the fact that we do not have any data upon which the model can be optimized with respect to pH as an independent variable.

Using Eq. (13) [6], the diffusivity of the oxygen anion vacancy (the presumed dominant point defect on defective Zirconia) in the passive film formed in the above high temperature, de-aerated borate buffer solution, D, is calculated to be in the range from 8.61×10^{-14} cm^2/s to 1.02×10^{-13} cm^2/s within the experimental applied potential range. The level of agreement between the diffusivity derived in this work and that measured in high temperature, solid state experiments [14–17] is reasonable, as shown in Fig. 3

$$D = 2\sigma^2(1-\alpha)^2 I_{ss}^2/\varepsilon^2. \tag{13}$$

From Eq. (14), the polarization resistance, R_p, is calculated to be 4071, 5211 and 4940 Ω at 0.4, 0.5 and 0.6 V_{SHE}, respectively, in the high temperature, de-aerated borate buffer solution, where

$$R_p = Z(\omega = 0) - Z(\omega = \infty). \tag{14}$$

The calculation indicates that the polarization resistance does change significantly with the porosity and thickness of the outer layer, but it varies little with applied voltage, the polarizability of

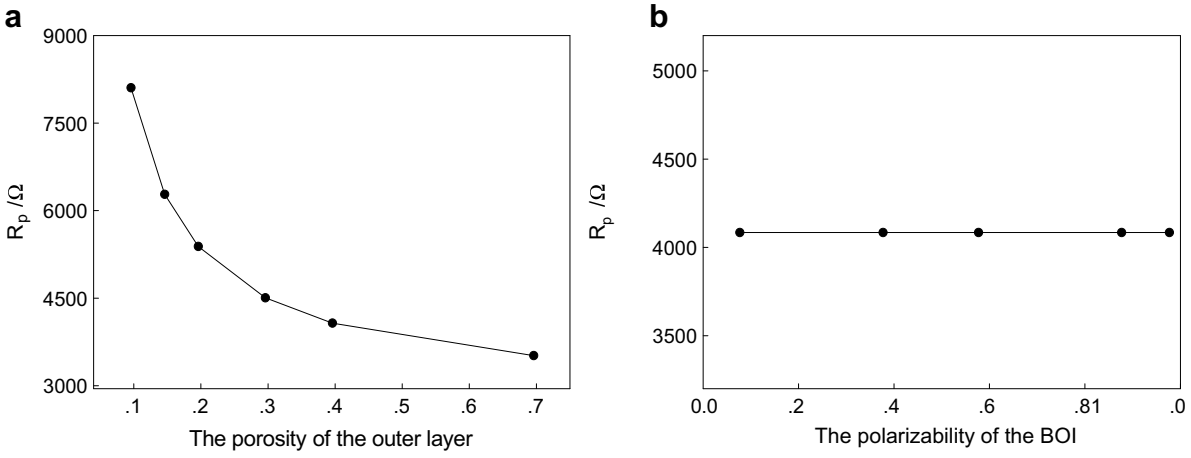

Fig. 4. Dependence of the R_p at 0.4 V_{SHE} on (a) the porosity of the outer layer, (b) the polarizability of the barrier layer/outer layer interface.

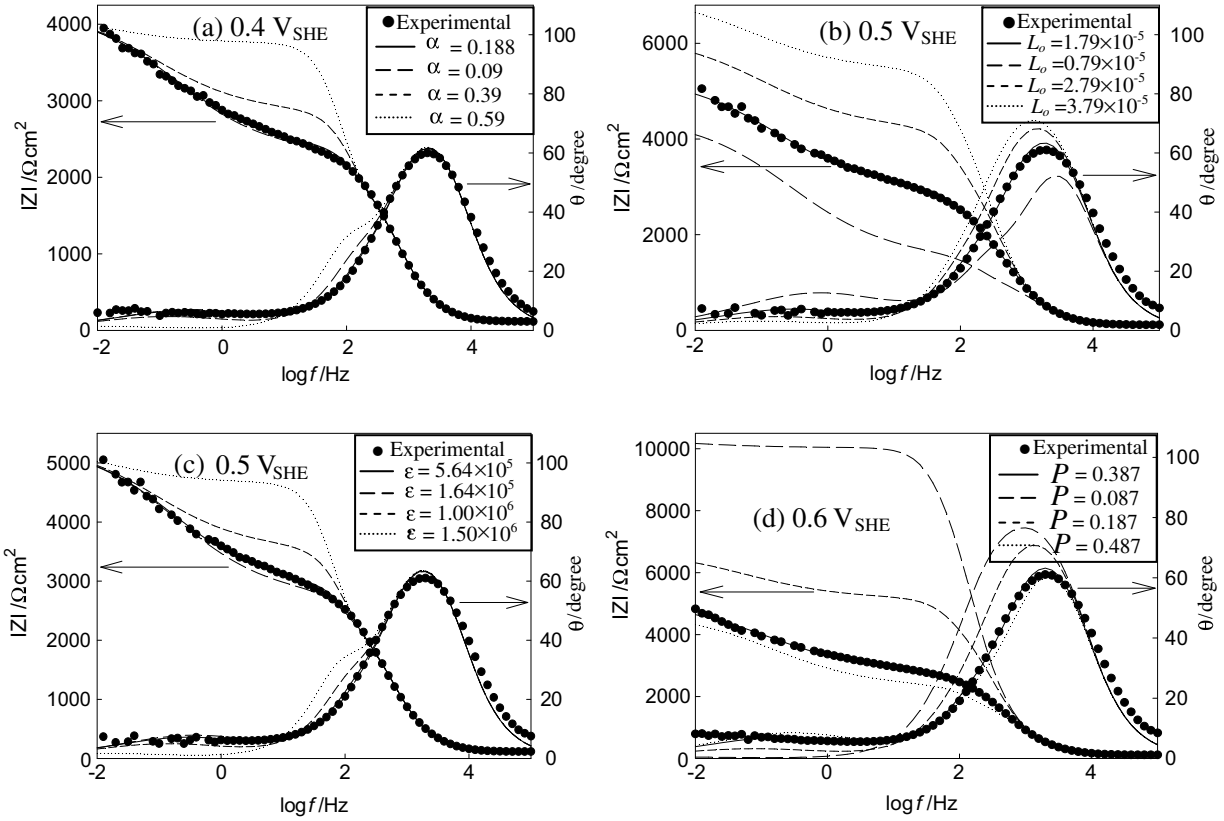

Fig. 5. Sensitivity analysis, showing the effect of model parameter value changes on the calculated impedance spectra in comparison with the measured spectra, where the solution is 0.1 M $B(OH)_3$ + 0.001 M LiOH at 250 °C, pH 6.94.

the BOI, the transfer coefficients, and the electric field strength across the barrier layer. Typical dependence of R_p on model parameter values are shown in Fig. 4, in which all other model parameter values are the same as those shown in Table 2. These data indicate that the corrosion resistance of zirconium in the de-aerated aqueous solution is dominated by the outer layer.

4.3. Sensitivity analysis

In order to rank the model parameters that have the greatest impact on the predictions of the model, extensive sensitivity analysis was carried out. Typical effects of changing the model parameter values on the calculated spectra are shown in Fig. 5, in which the other model parameter values are the same as those shown in Table 2. Also plotted in this figure are the experimental impedance data. It can be seen from this figure that the change of the porosity and thickness of the outer layer with reference to the results listed in Table 2 leads to the greatest deviation of the fitting curves from the experimental results, which indicates again that the corrosion resistance is dominated by the outer layer.

5. Summary and conclusions

In the present work, we developed an impedance model based on the point defect model for the growth of bi-layer passive films formed on zirconium under high temperature de-aerated aqueous solution conditions, and extracted values for various model parameters based on the experimental impedance data measured in high temperature, de-aerated aqueous solutions (0.1 M $B(OH)_3$ + 0.001 M LiOH, pH 6.94) at 250 °C. The principal findings of this work are as follows:

- The impedance model based on the PDM provides a reasonable account of the growth of bi-layer passive films formed on zirconium under the de-aerated aqueous solution conditions.
- The corrosion resistance of zirconium in high temperature, de-aerated aqueous solutions is dominated by the outer layer.
- The porosity of the outer layer, the electric field strength across the barrier layer, the polarizability of the barrier layer/outer layer interface, the standard rate constants and transfer coefficients for the point defect generation and annihilation at the barrier layer interfaces, and other parameters are found to be essentially constant within the applied potential range explored in this work.
- The extracted model parameter values can be used in deterministic models for predicting the accumulation of general corrosion damage to zirconium.

Acknowledgements

The authors gratefully acknowledge the support of the US Department of Energy through Grant No. DE-FG03-02SF-22618.

References

[1] D.D. Macdonald, A. Sun, N. Priyantha, J. Electroanal. Chem. 572 (2004) 421.
[2] D. Feron, D. Crusset, J.M. Gras, J. Nucl. Mater. 379 (2008) 16.
[3] D.D. Macdonald, J. Mankowski, M. Karaminezhaadranjbar, Y.H. Hu, Corrosion 44 (1988) 186.
[4] Y. Chen, M. Urquidi-Macdonald, D.D. Macdonald, J. Nucl. Mater. 348 (2006) 133.
[5] D.D. Macdonald, J. Electrochem. Soc. 139 (1992) 3435.
[6] C.Y. Chao, L.F. Lin, D.D. Macdonald, J. Electrochem. Soc. 128 (1981) 1187.

[7] L. Zhang, D.D. Macdonald, E. Sikora, J. Sikora, J. Electrochem. Soc. 145 (1998) 898.
[8] M. Urquidi-Macdonald, S. Real, D.D. Macdonald, Electrochim. Acta 35 (1990) 1559.
[9] M. Urquidi-Macdonald, S. Real, D.D. Macdonald, J. Electrochem. Soc. 133 (1986) C132.
[10] I. Betova, M. Bojinov, T. Laitinen, K. Makela, P. Pohjanne, Corros. Sci. 44 (2002) 2675.
[11] J.H. Ai, Y.Z. Chen, M. Urquidi-Macdonald, D.D. Macdonald, J. Electrochem. Soc. 154 (2007) C52.
[12] Anon, Waterside Corrosion of zirconium Alloys in Nuclear Power Plants, IAEA-TECDOC-996 (1998).
[13] O. Pensado-Rodriguez, J.R. Flores, M. Urquidi-Macdonald, D.D. Macdonald, J. Electrochem. Soc. 146 (1999) 1326.
[14] P.S. Manning, J.D. Sirman, R.A. De Souze, J.A. Kilner, Solid State Ionics 100 (1997) 1.
[15] H. Solmon, Autodiffusion de l'oxygene, du zirconium et de l'yttrium dans la Zircone Cubique Stabilisee par l'yttrium", PhD Thesis, Universite Paris, 1992.
[16] M. de Ridder, R.G. van Welzenis, H.H. Brongersma, U. Kreissig, Solid State Ionics 158 (2003) 67.
[17] M. Bojinov, L. Hansson-Lyyra, P. Kinnunen, T. Saario, P. Sirki, J. ASTM Int. 2 (2005) 1.